Footprint and detectability of a well leaking CO_2 in the Central North Sea: Implications from a field experiment and numerical modelling

Lisa Vielstädte[a,*], Peter Linke[a], Mark Schmidt[a], Stefan Sommer[a], Matthias Haeckel[a], Malte Braack[b], Klaus Wallmann[a,*]

[a] *GEOMAR Helmholtz Centre for Ocean Research Kiel, Germany*
[b] *Department of Applied Mathematics, University of Kiel, Germany*

ABSTRACT

Existing wells pose a risk for the loss of carbon dioxide (CO_2) from storage sites, which might compromise the suitability of carbon dioxide removal (CDR) and carbon capture and storage (CCS) technologies as climate change mitigation options. Here, we show results of a controlled CO_2 release experiment at the Sleipner CO_2 storage site and numerical simulations that evaluate the detectability and environmental consequences of a well leaking CO_2 into the Central North Sea (CNS). Our field measurements and numerical results demonstrate that the detectability and impact of a leakage of $< 55\,t\,yr^{-1}$ of CO_2 would be limited to bottom waters and a small area around the leak, due to rapid CO_2 bubble dissolution in seawater within the lower 2 m of the water column and quick dispersion of the dissolved CO_2 plume by strong tidal currents. As such, the consequences of a single well leaking CO_2 are found to be insignificant in terms of storage performance. Only prolonged leakage along numerous wells might compromise long-term CO_2 storage and may adversely affect the local marine ecosystem. Since many abandoned wells leak natural gas into the marine environment, hydrocarbon provinces with a high density of wells may not always be the most suitable areas for CO_2 storage.

1. Introduction

Geological storage of carbon dioxide (CO_2) aims at reducing the amount of anthropogenic CO_2 added to the atmosphere (e.g. Metz et al., 2005) and plays a role in various carbon dioxide removal techniques that have been proposed to reduce the CO_2 content of the atmosphere (IPCC, 2014). In Europe, the largest potential to store CO_2 is offshore (~ 240 Gt of CO_2) mostly in deep saline aquifers (e.g. EU GeoCapacity, 2009). More than 80% of the European offshore storage capacity is located in Norwegian waters (EU GeoCapacity, 2009), where Statoil operates the world's first large-scale CO_2 storage project "Sleipner" with an annual injection rate of ~ 1 Mt of CO_2 since 1996 (Fig. 1). Here, CO_2 from natural gas production is injected into a saline aquifer in ~ 900 m sediment depth, overlying the geological gas reservoir where it is extracted from (Torp and Gale, 2004; Arts et al., 2008). As such, Sleipner and many other large-scale CO_2 storage projects are located in regions that have already been exploited for hydrocarbon production. This has several benefits as compared to undeveloped sites: 1) they tend to be geologically well-understood with existing wellbore and seismic data helping to characterize the local geology and overburden, and 2) may

already have infrastructure in place (Jordan et al., 2015). One downside of storing CO_2 in developed sites is the presence of pre-existing wells (Gasda et al., 2004; Nordbotten et al., 2005), which have been identified for posing a greater risk for gas leakage from CO_2 storage formations than natural geological features, such as faults or fractures (Bachu and Watson, 2009). However, so far, there is no evidence for CO_2 leakage through wells, faults, and the overburden at Sleipner (Eiken et al., 2011; Chadwick et al., 2009) indicating that CO_2 is safely contained within the storage complex.

Concern about CO_2 leakage along abandoned wells is widely attributed to well barrier failures (Gasda et al., 2004; Nordbotten et al., 2005; OSPAR Convention, 2007; EU CCS Directive GD1, 2011), where CO_2 may escape from the storage reservoir either due to pre-existing failures in the well material or due to subsequent corrosion of the cement and steel casings that are exposed to the subsurface CO_2 plume (Kutchko et al., 2007; Carey et al., 2010, 2007; Crow et al., 2010), but were originally not designed to withstand CO_2 (Bachu and Watson, 2009). Estimates on CO_2 gas flows associated to this kind of leakage are low: 0.1 kg yr^{-1} for leakage along a well with degraded cement (Jordan et al., 2015), less than 0.1 t yr^{-1} for leakage along a well with sustained
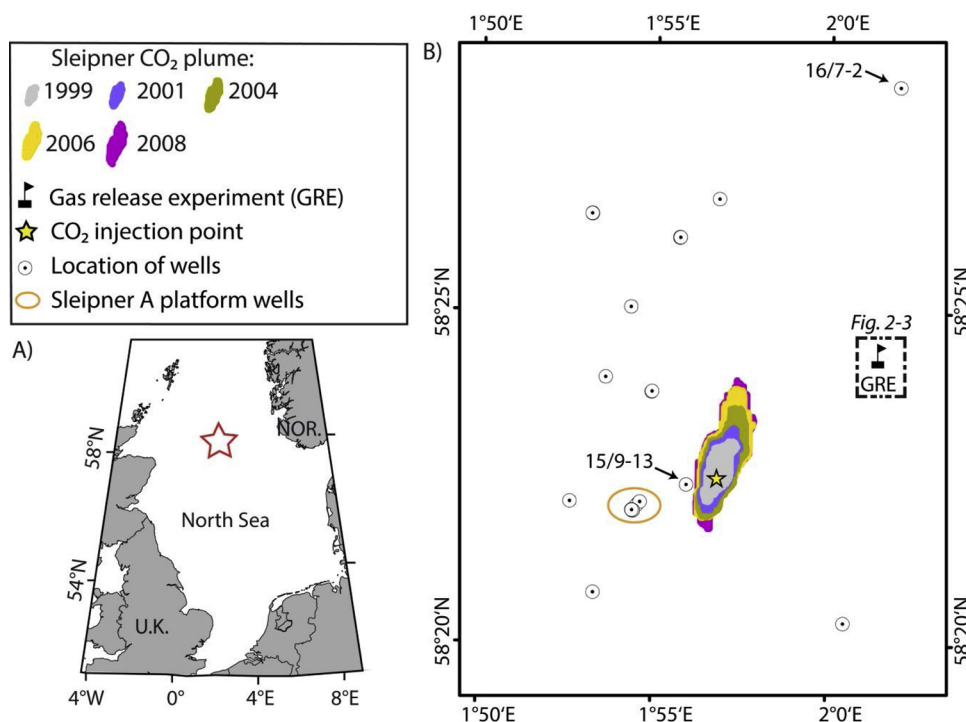
Fig. 1. A) Overview map showing the location of the study area (red star) in the CNS. B) Map of the study area showing the Sleipner CO_2 injection point (yellow star), the predominantly north-eastward extension of the CO_2 plume within the ~900 m deep Utsira sand formation (colored contours), the location of the gas release experiment (GRE, black flag, 58°24′22.41″N, 2°1′25.54″E), and the location of wells (circles) in the area. Platform wells (orange circle) from which the CO_2 is injected and those which have been identified to leak shallow gas (wells 15/9-13 and 16/7-2, Vielstädte et al., 2015) are highlighted.

casing pressure (Tao and Bryant, 2014), and 0.3–3 t yr^{-1} for poorly cemented wells (Jordan et al., 2015) with a typical wellbore cement permeability below 1 Darcy (Crow et al., 2010). Higher leakage rates, on the order of 3–52 t yr^{-1} of CO_2 (Vielstädte et al., 2015, 2017; Bachu, 2017), may arise from gas losses along the outside of wells, where drilling has disturbed and fractured the sediment around the wellbore mechanically thereby creating highly efficient pathways for the upward migration of gas (Gurevich et al., 1993). This kind of leakage has recently been observed at abandoned gas wells in the CNS, where biogenic methane, originating from a shallow (< 1000 mbsf) gas source in the sedimentary overburden above the deep hydrocarbon reservoirs, leaks into seawater (Vielstädte et al., 2015; 2017). Shallow gas leakage is presently not targeted by regulatory frameworks except in Alberta (Canada), but may have important implications for CO_2 storage in developed hydrocarbon provinces with high well density especially in shallow strata above deeper hydrocarbon reservoirs.

Here, we focus on the Sleipner CO_2 storage site (Fig. 1A) and investigate hypothetic, but realistic leakage of CO_2 along a well that penetrates the subsurface CO_2 plume and leaks into the ~80 m deep water column, using a combination of experimental field data and numerical modelling. The main objectives of this study are to predict the spatial footprint, detectability, and environmental consequences of a well leaking CO_2 at realistic rates and under real tidal forcing by analyzing an existing bubble dissolution model and a newly developed plume dispersion model against the data collected from an *in situ* CO_2 leakage experiment. Results presented in this study are directly applicable to most global offshore CO_2 storage sites, which are planned for hydrocarbon provinces, where ubiquitous hydrocarbon infrastructures pose a risk for the upward migration of gas. This study further fills a gap in CO_2 storage-related field experiments and hydrodynamic modelling research, which mostly operated at large scales and high rates addressing the release of CO_2 during a highly unlikely blowout scenario (Phelps et al., 2014; Dewar et al., 2013; Hvidevold et al., 2015; Greenwood et al., 2015; Dissanayake et al., 2012) and leaky fault scenario (Kano et al., 2010) or have investigated leakage at low rates into shallow coastal waters (i.e. QICS experiment; Blackford et al., 2014; Dewar et al., 2015; Mori et al., 2015; Sellami et al., 2015), with hydrodynamic properties that are not representative for submarine

storage projects that are operating or are under consideration in the open North Sea.

2. Materials and methods

During the Celtic Explorer expedition CE12010 (July-August 2012), a controlled gas release experiment (GRE) was conducted at 81.8 m water depth to simulate leakage of CO_2 into the North Sea water column in the vicinity of the Sleipner CO_2 storage site (Fig. 1, section 2.1). A gas bubble dissolution model (BDM; Vielstädte et al., 2015) was applied to calculate the rate of CO_2 dissolution in seawater (section 2.2). The resulting rate was used as input parameter for the plume dispersion model (PDM) that was applied to simulate the spread of dissolved CO_2 in the water column (section 2.3). Both models were calibrated against the observational GRE data (section 2.4). Subsequently, the calibrated models were applied to compute three leaky well scenarios covering the range of possible emission rates (section 2.5).

2.1. Gas release experiment (GRE)

Three pressure bottles of CO_2 (50 L, 57 bar), one smaller bottle of Krypton (10 L, 250 bar), which was used as a tracer gas, two battery packs, a gas control unit, and release head, were mounted to the Lander system ("Ocean Elevator", Linke et al., 2015) and deployed video-guided at the seafloor (58°24′22.41″N, 2°1′25.54″E, Fig. 2). The control unit included a spiral coil and a heated pressure regulator to reduce the pressure of the outflowing gas from up to 250 bar inside the gas bottle to 11 bar before the gas entered the microcontroller, which regulated the gas flow (Fig. 2C). Bubbles were generated on top of the Ocean Elevator by seven 1/8" stainless steel tubes connected by valves and covered by plastic heads which were pierced by three 8 mm holes each (Fig. 2B). At a preset gas flow of 30 L min^{-1} at STP (25 °C, 1 bar), a total of 40 kg of CO_2 was released into the water column over a period of 11.5 h. This corresponds to an annual leakage rate of 31 t yr^{-1} of CO_2, which falls in the upper range of methane gas fluxes observed at abandoned wells in the CNS (Vielstädte et al., 2015).

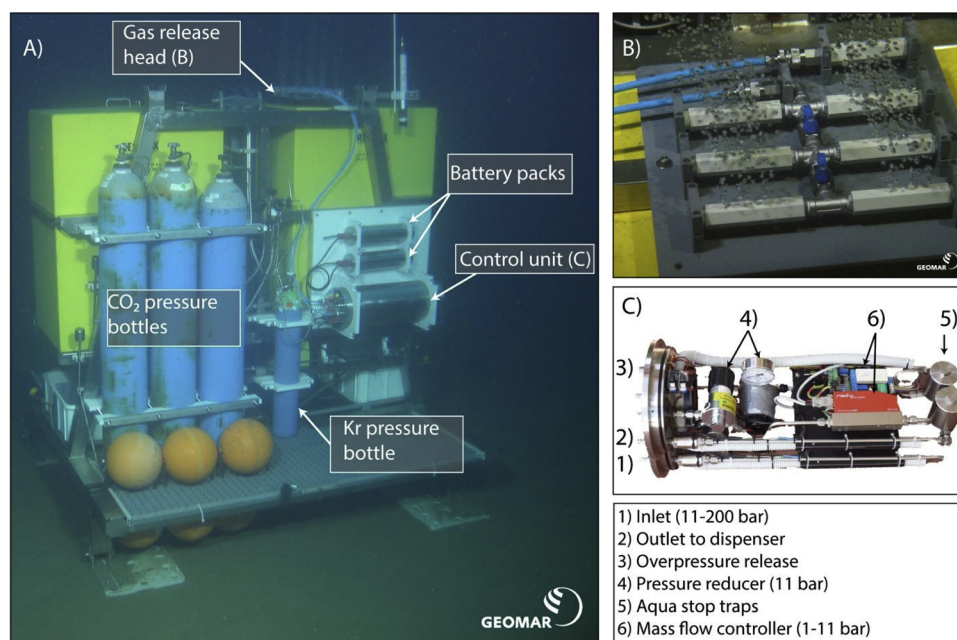The gas discharge was observed in situ during a 4 h dive with the

Fig. 2. Gas release experiment (GRE). A) Picture showing the setup of the GRE, i.e. the Ocean Elevator (with yellow syntactic foam blocks) and mounted equipment, deployed at ~80 m water depth in the vicinity of the Sleipner CO_2 storage site. B) Single CO_2 bubble streams were released from the gas release head on top of the Ocean Elevator (in addition Krypton (Kr), used as a tracer gas, was released from the single tube in the back). C) Set-up of the gas control unit, regulating the pressure and gas flow during the experiment.

remotely operated vehicle ROV Kiel 6000 (GEOMAR Helmholtz-Zentrum für Ozeanforschung Kiel, 2017) equipped with HD camera/video device and a sonar system. The sonar system was used to navigate the ROV downstream of the artificial CO_2 leak by tracking the less soluble and ~27 m high Krypton gas flare. The spread of the dissolved CO_2 plume was monitored geochemically using the commercial HydroC pCO_2 sensor (S/N 0412-006, Kongsberg Maritime Contros GmbH) mounted to the front porch of the ROV. The sensor was calibrated for pCO_2 signals up to 3000 µatm (accuracy ~1% of reading resolution; resolution: < 30 µatm as described by Fietzek et al., 2014) and was programmed to measure in 60 s intervals, which is equal to the sensor's response time (Fiedler et al., 2013). For a better navigation of the ROV in the plume, HydroC sensor data were, in addition to internal data recording, transferred as an analog voltage signal which enabled online reading of the pCO_2 signal during ROV operation. ROV-operated pCO_2 surveying was performed in different vertical heights and distances downstream of the artificial leak, remaining at each measuring position for at least 10 min to obtain a representative pCO_2 signal. At the end of the experiment a vast number of hagfish visited the release site, potentially attracted by the smell of dead meio- and macrofauna in the sediment. Unfortunately, ship time was too limited to study this phenomenon in more detail.

The initial bubble size distribution (ψ), produced during the experiment, was determined from ROV HD images applying the image editing software ImageJ (Farreira and Rasband, 2012). For calibration of bubble sizes, the length of the gas releaser tube (10 cm) was used as scale. Ellipses were manually overlaid to individual bubbles leaving the top of the Ocean Elevator and were marked as overlays. If bubbles had a very irregular shape, they were outlined manually before using the ellipse fitting object of ImageJ. The corresponding bubble volume, $V_0 = 4/3 \cdot \pi \cdot r_{eq}^2$, was calculated from the equivalent spherical radius, $r_{eq} = (a^2 \cdot b)^{1/3}$ based on the major, a, and the minor half axes, b, of the fitted ellipse. All determined bubble volumes were added to calculate the total gas volume (V_ψ) and the volumetric contribution of each bubble size class (i.e. V_0/V_ψ), both required to calculate the CO_2 bubble dissolution rate into seawater during the experiment. The accuracy of bubble size measurements was better than 0.2 mm as determined from the HD image resolution of 55.1 pixels cm^{-1} and a measurement precision of 1 pixel.

Current velocities and directions were recorded during two deployments (OCE1 and OCE2) using an Acoustic Doppler Current

Profiler (ADCP, Teledyne RD Instruments) operating at 300 kHz. The vertical resolution of the ADCP was set to 1 m with the first bin starting 3.2 m above the seafloor (masf). OCE1 was a long-term deployment measuring currents over several tidal cycles (i.e. 5 days) that was used to characterize the regional flow field (58.4054 °N, 2.0221 °E) and parameterize the leaky well scenarios, whereas OCE2 was a short-term deployment at the experimental site recording currents 28 m to the east of the Ocean Elevator during the time of the gas release experiment (ADCP measurements during OCE1 and OCE2 can be downloaded from the links: https://doi.pangaea.de/10.1594/PANGAEA.833751, https://doi.pangaea.de/10.1594/PANGAEA.833761).

The ROV data set including positioning data (longitude, latitude and water depth) was combined with data derived from HydroC-CO_2 and ADCP measurements by correlating their UTC time stamps. The combined dataset was mapped using the geographic information system software ArcGIS v.10.1 (Fig. 3A). For comparison with numerical predictions, pCO_2 data were averaged over periods of equal ROV positioning (i.e. 10 min).

2.2. Gas bubble dissolution model (BDM)

An existing BDM (Vielstädte et al., 2015, 2017) was used to calculate the dissolution rate of CO_2 bubbles in seawater by a single rising gas bubble. The model simulates the shrinking of a gas bubble due to dissolution in the water column, its expansion due to decreasing hydrostatic pressure in the course of its ascent and gas stripping. The BDM uses finite difference methods implemented in the NDSolve object of Mathematica (i.e. LSODA, Sofroniou and Knapp, 2008) solving a set of coupled ordinary differential equations describing these processes for each of the involved gas species (CO_2, N_2, and O_2) and the bubble rise velocity (Wüest et al., 1992). Thermodynamic and transport properties of the gas components, such as molar volume (Duan et al., 1992), gas compressibility (Duan et al., 1992), and gas solubility in seawater (Duan et al., 2006), were calculated from respective equations of state, and empirical equations for diffusion coefficients (Boudreau, 1997), mass transfer coefficients (Zheng and Yapa, 2002), and bubble rise velocities (Wüest et al., 1992), taking into account local pressure, temperature and salinity conditions as measured by CTD casts. A detailed description of the model can be found in Vielstädte et al., 2015 and 2017.

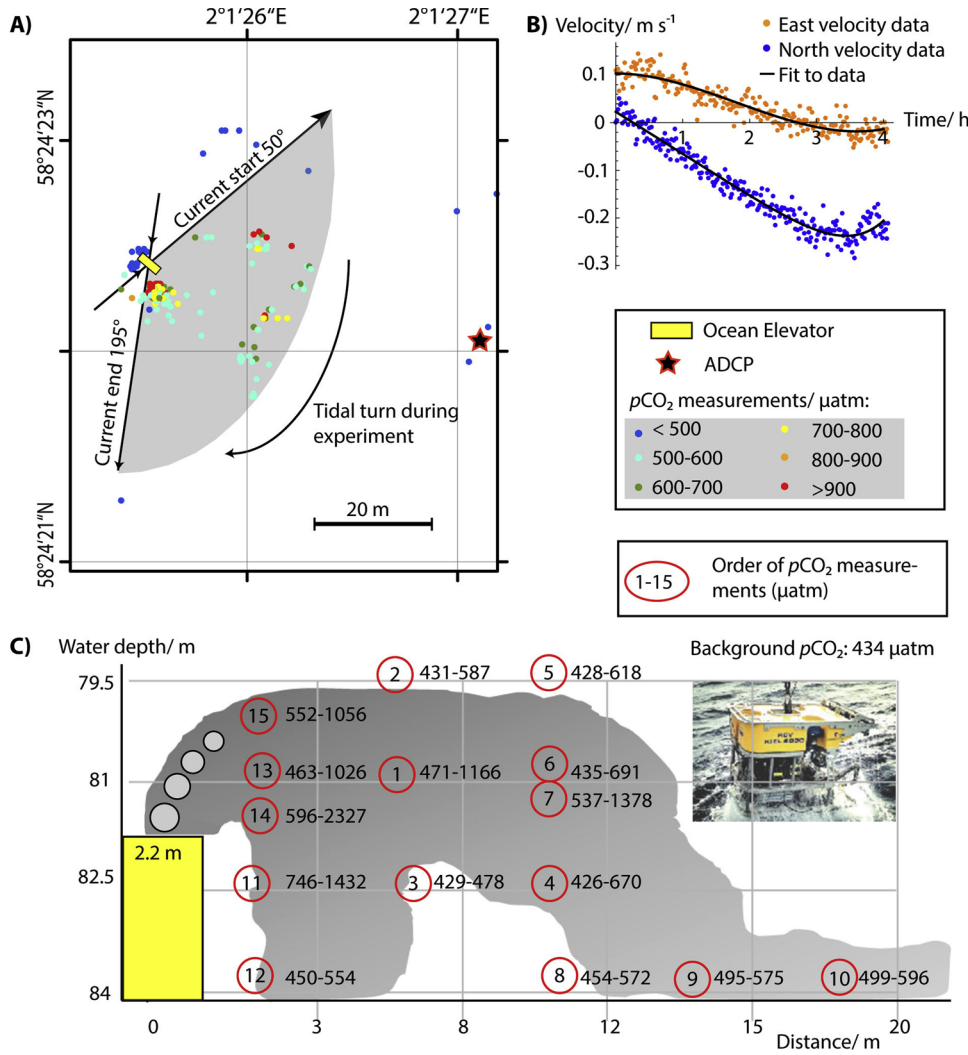Model boundary conditions and parameterizations (Table 1) were

Fig. 3. A) Distribution map of pCO_2 measurements (colored circles) during the 4 h ROV observation of the GRE showing the different current flow angles towards the Ocean Elevator (yellow box) when the tide turned and the location of the ADCP (black star) 28 m to the east of the GRE. Background pCO_2 values (blue dots) were measured upstream of the tidal current before the GRE started (background values measured during the ROV survey when the ROV was not downstream of the CO_2 plume have been excluded from the plot). B) ADCP measurements of current velocities in eastern (orange dots) and northern (blue dots) directions at 3.2 m above the seafloor during the 4 h ROV observation of the GRE. C) Scheme illustrating the order (red circles) and magnitude (black values) of pCO_2 measurements and down-welling of the CO_2 plume as measured downstream of the Ocean Elevator.

obtained from Sea-Bird 9 plus CTD data from July 2012 and run for different initial bubble sizes (r_0) ranging between 1 to 4 mm radius, in accordance to radii observed during the gas release experiment and at North Sea wells leaking methane (Vielstädte et al., 2015). The simulated water depth was defined as 81.8 m in accordance to that of the GRE and depths important for CO_2 leakage from the seafloor in the Sleipner area. The CO_2 background concentration in ambient seawater of 0.021 mM (or 434 µatm) was determined from HydroC-pCO_2 measurements at the GRE site prior to the gas release while dissolved O_2 concentrations of 0.235 mM were determined at well 15/9-13 (Linke, 2012). Dissolved N_2 was considered to be in equilibrium with the atmospheric partial pressure due to a lack of water column measurements.

For a given initial bubble radius (r_0), the CO_2 dissolution rate (R in mol s^{-1}) was determined numerically by the BDM. After numerical computation, R was normalized to the initial bubble CO_2 content (N_0 in mol) and divided by the corresponding bubble rise velocity (v_b in m s^{-1}) to calculate the normalized bubble dissolution rate (BD in m^{-1}) as a function of the bubble distance from the seafloor (z):

$$BD(r_0, z) = \frac{R(r_0, z)/N_0}{v_b(r_0, z)} \left[\frac{1}{m} \right]$$

(1)

Because our experiment and methane leaking wells in the North Sea (Vielstädte et al., 2015) expelled a range of initial bubble sizes, the CO_2 bubble dissolution rate BD (r_0,z) was calculated for each initial bubble size and weighted by its volumetric contribution, V_0, to the total

emitted gas bubble volume, V_ψ. Integrating this weighted bubble dissolution rates over the entire initial bubble size spectrum (ψ) gives the total CO_2 dissolution rate (BD(ψ,z)) as a function of the bubble distance from the seafloor and with respect to the initial CO_2 released at the seafloor (Vielstädte et al., 2015, Fig. 4A):

$$BD(\psi, z) = \frac{1}{MI} \int_{r(\min)}^{r(\max)} BD(r_0, z) \cdot \frac{V_0}{V_\psi} dr \left[\frac{1}{m} \right]$$

(2)

where, r(min) and r(max) are the minimum and maximum bubble sizes of the total spectrum, respectively, and MI is the measurement interval between individual bubble sizes (i.e. 0.1 mm), both determined from HD images of the bubble release.

It should be noted that the applied BDM is valid for the release of single bubble streams but not necessarily for bubble plumes which involve additional dynamics (e.g. upwelling of entrained water, bubble rise paths deviating from a straight upward direction). Hence, this study is not meant to capture the physics of overpressure-driven leakage of CO_2, such as blowout accidents, which likely involves much larger leakage rates and complex bubble plume dynamics (e.g., Schneider von Deimling et al., 2015). In this study, the simulation of a single rising bubble seems to be justified because leakage along wells is driven by buoyancy-controlled gas migration (Vielstädte et al., 2015). Enhanced bubble rise velocities have not been observed at methane leaking wells in the North Sea, neither at low nor at high tide (Vielstädte et al., 2015). This is in contrast to the QICS CO_2 injection experiment, where individual bubbles in Scottish shallow waters rose faster due to bubble

Table 1
Parameterization of the bubble dissolution model.

Parameter values/Equations	Range	Variance	Reference
[a]Diffusion coeff.: D_i / $m^2\ s^{-1}$			
$D_{O2} = 1.05667 \cdot 10^{-9} + 4.24 \cdot 10^{-11} \cdot T$	T:0-25 °C	$1.00 \cdot 10^{-21}$	Boudreau, 1997
$D_{N2} = 8.73762 \cdot 10^{-10} + 3.92857 \cdot 10^{-11} \cdot T$	T:0-25 °C	$2.94 \cdot 10^{-23}$	Boudreau, 1997
$D_{CO2} = 8.38952 \cdot 10^{-10} + 3.8057 \cdot 10^{-11} \cdot T$	T:0-25 °C	$4.76 \cdot 10^{-25}$	Boudreau, 1997
Mass transfer coefficient: $K_{L,i}$ / $m\ s^{-1}$			
$K_L = 0.013 \cdot (v_b\ 10^2/(0.45 + 0.4 \cdot r \cdot 10^2))^{0.5} \cdot D_i^{\ 0.5}$	r ≤ 2.5 mm		Zheng and Yapa, 2002
$K_L = 0.065 \cdot D_i^{\ 0.5}$	2.5 < r ≤ 6.5 mm		Zheng and Yapa, 2002
$K_L = 0.0694 (2 \cdot r \cdot 10^2)^{-0.25} \cdot D_i^{0.5}$	r < 6.5 mm		Zheng and Yapa, 2002
Fit to CTD data as function of the water depth (z_{sw})			
$T(z_{sw}) = 8 + 7/(1 + e^{\ 0.375\ (-21.7512\ +\ zsw)})$ [°C]	Z_{sw}: 0-100 m	$3.99 \cdot 10^{-2}$	CE12010 45-CTD12
$S(z_{sw}) = 35.12 - 0.67/(1 + e^{\ 0.4125\ (-20.1595\ +\ zsw)})$ [PSU]	Z_{sw} : 0-100 m	$4.97 \cdot 10^{-4}$	CE12010 45-CTD12
Density of sea water: φ_{SW}/ $kg\ m^{-3}$			
$\varphi_{SW}(z_{sw}) = 1027.7 - 2.150/$	Z_{sw} : 0-100 m	$6.8 \cdot 10^{-3}$	Unesco, 1981
$(1 + e^{\ 0.279\ (-21.612 + zsw)})$			
Bubble rise velocity: vb / $m\ s^{-1}$			
$v_b = 4474 \cdot r^{1.357}$	r < 0.7 mm		Wüest et al., 1992
$v_b = 0.23$	0.7 ≤ r < 5.1 mm		Wüest et al., 1992
$v_b = 4.202 \cdot r^{0.547}$	r ≥ 5.1 mm		Wüest et al., 1992
Gas solubility: c_i / mM			
$cN_2 = 0.622 + 0.0721 \cdot z_{sw}$	Z_{sw} :0-100 m	$2.5 \cdot 10^{-3}$	Mao and Duan, 2006
$cO_2 = 1.08 + 0.1428 \cdot z_{sw}$	Z_{sw} :0-100 m	$9.8 \cdot 10^{-3}$	Geng and Duan, 2010
$cCO_2 = (0.041 + 0.00476 \cdot z_{sw}) \cdot \varphi_{SW}$	Z_{sw} :0-100 m	$5.7 \cdot 10^{-5}$	Duan et al., 2006
CO_2 molar volume: $MVCO_2$ / $L\ mol^{-1}$			
$MVCO_2 = 1/(0.04 + 0.00458 \cdot z_{sw})$	Z_{sw} :0-100 m	0.1	Duan et al., 1992
Hydrostatic Pressure: P_{hydro}/ bar			
$P_{hydro} = 1.013 + \varphi_{SW} \cdot g \cdot z_{sw}$			

[a] The parameterization of the diffusion coefficients is based on a seawater salinity of 35. Pressure effects have been neglected because the resulting error is < 1% at < 100 m water depth.

plume dynamics (upwelling; Sellami et al., 2015; Dewar et al., 2015). Due to the larger gas flux in our gas release experiment compared to that observed at methane leaking wells, we cannot explicitly exclude that bubbles rose in the absence of plume dynamics during our experiment (Supplementary video data of our experiment can be downloaded from the link: https://www.pangaea.de/tok/e3a4d8996affba87b666c04d969672657c32313d). However, we here restrict ourselves by modelling the dissolution rate of a single rising bubble without considering effects like upwelling and entrainment of water due to the overall good agreement of modelling results and data (i.e. measurements of pCO$_2$ and the maximum CO$_2$ bubble rise height coincide well with modelling results; see Section 3.1.). Other plume dynamics, such as turbulence (Leifer et al., 2015), and/or spiral movement (Schneider von Deimling et al., 2015), which have been observed at other bubble plumes and counter act a reduced bubble dissolution rate induced by upwelling, may explain the good fit of our simulation results to experimental data.

2.3. Plume dispersion model (PDM)

The model uses the COMSOL module "Transport of Diluted Species"

(tds) for chemical species transport via diffusion and advection in a turbulent flow (i.e. Re > 2000 for the North Sea) that is based on the general mass balance equation:

$$\frac{\partial C}{\partial t} = \nabla \bullet ([D_M + D_T] \nabla C - u\,C) + S\,[\frac{mol}{m^3\,s}] \qquad (3)$$

where, C is the concentration of the dissolved species (here dissolved inorganic carbon (DIC) in mol m^{-3}), t is the time (s), the Nabla operator ∇ refers to the derivatives with respect to the spatial coordinates x,y, and z , u is the current velocity vector (m s^{-1}), D denotes the diffusion coefficient including a molecular (D_M) and a turbulent diffusion component (D_T) (m^2 s^{-1}), and S is the source term of DIC production (mol m^{-3} s^{-1}) resulting from CO$_2$ bubble dissolution expressed as 2-D Gaussian distribution:

$$S = \frac{1}{\pi \bullet w} e^{-(\frac{x^2+y^2}{w})} \bullet R_{CO2} \bullet BD(\psi, z)[\frac{mol}{m^3\,s}] \qquad (4)$$

where, w denotes the area (m^2) of the Gaussian pulse in x and y direction, R_{CO2} is the rate of CO$_2$ gas bubble release (mol s^{-1}) from the seafloor, and $BD(\psi,z)$ is the normalized rate of CO$_2$ bubble dissolution as determined from the BDM (Eq. (2), Fig. 4B).

A) Bubble size distribution:
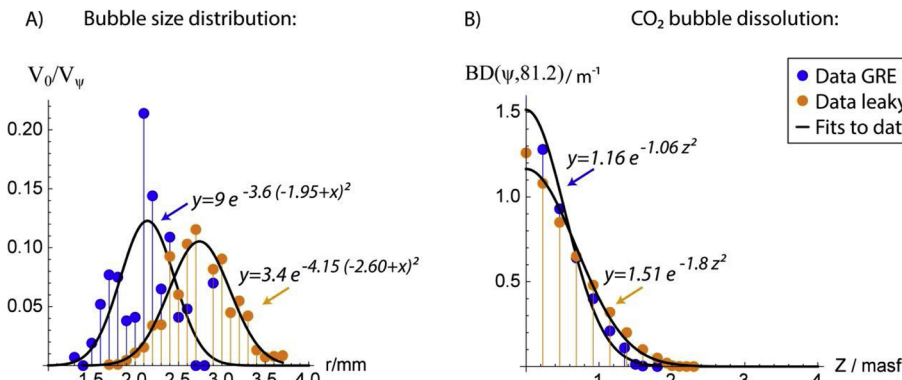
B) CO$_2$ bubble dissolution:

Fig. 4. A) Bubble size distributions measured during the GRE (blue dots) and at methane leaking wells in the CNS (orange dots, Vielstädte et al., 2015). B) Calculated rates of CO$_2$ bubble dissolution as a function of the distance to the seafloor (z) based on the initial bubble size distributions of the GRE (blue dots) and leaking wells in the CNS (orange dots). CO$_2$ bubbles dissolve within the lower 2 m of the water column. Details on the accuracy of data fits (black line) are given in the Supplementary Material.

The horizontal advective flow (u) in x and y direction is parameterized according to least-squares fits to ADCP velocity data measured at 3.2 masf and applying the Kármán–Prandtl "Law of the Wall" (LOW) describing the current velocity vector as a function of time (t) and distance from the seabed (z) (e.g. McGinnis et al., 2014):

$$u_x(t, z) = \frac{u_x^*(t)}{ka}\ln(\frac{z}{z_0}), \quad [\frac{m}{s}] \tag{5}$$

$$u_y(t, z) = \frac{u_y^*(t)}{ka}\ln(\frac{z}{z_0})$$

Where, u^* denotes the shear velocity in x and y direction calculated from ADCP data, z_0 is the roughness length ($1.4 \cdot 10^{-4}$ m for the North Sea; McGinnis et al., 2014) defining the height at which the current velocity tends to zero (Lefebvre et al., 2011), z is the distance to the seafloor, and ka is the dimensionless Kármán constant (0.4, Kundu and Cohen, 2008). As such, advective velocities are assumed to be horizontally, but not vertically and temporarily uniform. The vertical advection component is ignored because it is orders of magnitude smaller than the horizontal one.

Since the model uses least-squares fits to ADCP velocity data, small-scale fluctuations (eddies) in the turbulent flow are not explicitly resolved. The convective phenomenon of turbulent mixing is accounted for in the calculation of the species transport by using an added component of diffusion (D_T), which is expressed in dependency to z, ka and u_r^*, the shear velocity in resultant current direction (e.g. McGinnis et al., 2014):

$$D_T = ka \cdot u_r^* \cdot z \left[\frac{m^2}{s}\right] \tag{6}$$

Molecular diffusion (D_M) is calculated according to Boudreau (1997) as a function of temperature, pressure, and salinity and is on the order of 10^{-9} m^2 s^{-1}. Diffusion is assumed to be isotropic and hence, is the only mechanism transporting dissolved species vertically in the model domain. Equations and parameter values are provided in Tables 2 and 3 for the GRE and leaky well simulation settings, respectively.

To avoid numerical instabilities of the solution in the advection dominated leakage scenario, the COMSOL Model uses both, streamline-upwind (Galerkin method (SUPG), Do Carmo and Alvarez, 2003) and crosswind (Codina, 1998) stabilizing advection schemes, which add artificial diffusion in streamline and orthogonal direction to the advection vector of the advection-diffusion equation (Eq. 3). Numerical diffusivity was limited by defining a lower gradient limit (g_{lim} in mol m^{-4}) denoting the smallest concentration change across an element that is considered by stabilization. g_{lim} was defined as 3 mol m^{-3} weighted by the mesh element size (h) and has been determined from sensitivity analysis, i.e. increase of g_{lim} until the solution remains constant (numerical accuracy) while also ensuring sufficient numerical stability. The combination of using stabilizing advection schemes and a high-resolution non-uniform mesh including a local mesh refinement around the gas release where concentration gradients change rapidly ensured the model is well suited for maintaining sharp concentration

gradients while also ensuring sufficient numerical stability. Nonetheless, with the finite element stabilization method the tracer dispersion calculated by the model is somewhat enhanced by the artificial diffusion that was added to the model to obtain numerically stable results.

The time-dependent problem was solved by integration of the partial differential equation (i.e. Eq. (3)) in time according to the implicit backwards differentiated formula method of COMSOL Multiphysics (Press et al., 2007). The COMSOL Multiphysics solver automatically chooses appropriate numerical time steps which were set to be within a certain relative tolerance (i.e. 0.01) for the accuracy of the integration estimated during runtime (Press et al., 2007). The numerical performance (stability) was controlled after each model run by mass balance error (MBE) calculations, which were overall better than 2%.

The computed concentration of DIC, which is the sum of chemical species resulting when CO_2 dissolves in seawater ($[CO_2] + [HCO_3^-] + [CO_3^{2-}]$), is converted into carbonate system parameters of interest, i.e. pCO_2 and pH, applying an analytical solution (Zeebe and Wolf-Gladrow, 2001) assuming constant total alkalinity (TA) and applying physical parameter values (temperature, salinity, and pressure) obtained by CTD casts (Sea Bird 9 Plus) in July 2012 (Table 4). Total alkalinity of seawater was determined by titration with 0.02 N HCl using a mixture of methyl red and methylene blue as indicator. The titration vessel was bubbled with argon to strip any CO_2 produced during the titration. The IAPSO seawater standard was used for calibration; analytical precision and accuracy are both ~2%. TA is assumed to be constant during the GRE.

2.4. Simulating the gas release experiment

The first modelling case is designed to simulate the GRE over the 4 h period of ROV observation, for which the effects of the tidal turn on CO_2 dispersion are examined and compared to in situ pCO_2 measurements. The computational domain is set to be 50 × 50 × 20 m³, with a smaller rectangle (2.2 × 0.7 × 2.2 m³) in its center, which represents the geometry of the Ocean Elevator from which the CO_2 bubbles are released. The non-uniform finite element mesh has a spatial resolution of 0.075–1.75 m, with a finer element distribution of maximal 0.2 m in size around the gas release spot (further information on the model setup is given in the supplementary material).

The DIC source rate (S), resulting from vertical CO_2 bubble dissolution, is parameterized according to the preset gas flow (R_{CO2}) of 85 kg day^{-1} of CO_2 and the calculated bubble dissolution rate (BD) of the initial bubble size distribution (ψ with a peak radius of 2.1 mm) at a water depth of 81.8 m and ambient seawater conditions (Table 2).

In contrast to the plume dispersion model setup, where the current velocity is parameterized in the model domain according to ADCP measurements and the LOW towards the seabed, current velocities (and other convective parameters) around the Ocean Elevator were calculated numerically because the ADCP was deployed too far away (i.e. 28 m) from the experiment to resolve modifications in the turbulent flow that the obstacle of the Ocean Elevator induced. Generally, the

Table 2
Parameterization of the plume dispersion model for the GRE simulation setting.

GRE Parameter	Parameter values/Equations	Unit
*Resultant velocity as a function of time (t) in seconds	$u_r(t) = 120 + 0.0062 \cdot t - 36 \, Sin(\frac{\pi \cdot t}{8000})$	mm s^{-1}
Sand roughness height	$k_{seq} = 3.2$	μm
Turbulent intensity	$I_T = 0.05$	
Turbulent length scale	$L_T = 0.01$	m
*Rate of CO_2 bubble dissolution	$BD(\psi_{GRE}, 81.2) = IF[z < 2.21, \, 0, \, 7.6 \cdot e^{-0.31 \cdot z^2}]$	m^{-1}
Leakage rate	$R_{CO2} = 31$	t yr^{-1}
Area of the Gaussian pulse	$w = 0.3$	m^2

* Details on the accuracy of data fits and the correlation of fit parameters are provided in the supplementary material.

Table 3
Parameterization of the plume dispersion model for the leaky well simulations.

Parameter	Parameter values/Equations
[*]East velocity (m s^{-1}) as a function of time (t) and depth (z) above the seafloor	$u_x(t,z) = \dfrac{\left(0.37 - 2.21 \cdot Sin\left[\frac{\pi \cdot (t + 5279)}{22400}\right]\right)}{ka} \cdot Log\left[\frac{z}{z_0}\right]$
[*]North velocity (m s^{-1}) as a function of time (t) and depth (z) above the seafloor	$u_y(t,z) = \dfrac{\left(-2.52 - 3.94 \cdot Sin\left[\frac{\pi \cdot (t - 36019)}{22400}\right]\right)}{ka} \cdot Log\left[\frac{z}{z_0}\right]$
[*]Shear velocity (mm s^{-1}) at 3.2 masf as a function of time (t)	$u_r^*(t) = \sqrt{\left(-2.05 + 4.56\frac{Sin[\pi \cdot (t + 8065)]}{22400}\right)^2 + \left(1.84 + 0.65\frac{Sin \cdot [\pi \cdot (t + 23260)]}{22400}\right)^2}$
Turbulent diffusion coefficient (m^2 s^{-1})	$D_T(t,z) = ka \cdot u_r^*(t) \cdot 10^{-3} \cdot z$
Molecular diffusion coefficient (m^2 s^{-1})	$D_M(t) = 10^{-9}$
Roughness length (m)	$z_0 = 1.4 \cdot 10^{-4}$ (e.g. McGinnis et al., 2014)
Kármán constant	$ka = 0.4$ (Kundu and Cohen, 2008)
[*]Normalized rate of CO_2 bubble dissolution (m^{-1})	$BD(z) = 1.16 \cdot e^{-1.06 \cdot z^2}$
Leakage rate of CO_2 (t yr^{-1})	$R_{CO2} = 10, 20, 55$
Area of the Gaussian pulse (m^2)	$w = 0.5$

* Details on the accuracy of data fits and the correlation of fit parameters are provided in the supplementary material.

flow field behind an obstacle is suppressed and forms periodically swirling vortices. These effects were resolved by using a k-ε turbulence model implemented in COMSOL Multiphysics (i.e. the spf physics interface) which calculates the turbulent fluid flow numerically by solving the Reynolds-Averaged-Navier-Stokes-Equation (RANS).

Using the k-ε turbulence model, the advective flow acts in the direction of the Reynolds-averaged velocity and not in that of the real instantaneous velocity of the fluid in the field. As a result, small eddies of the turbulent flow are not explicitly resolved, having however, a pronounced effect on the species transport, as they cause additional mixing. Turbulent mixing is accounted for in the calculation of the species transport by using an added component of diffusion (D_T in addition to molecular diffusion) that is equal to the ratio of the turbulent kinematic viscosity v_T (m^2 s^{-1}) to the dimensionless turbulent

Table 4
Parameterization of the carbonate system sub-model.

Carbonate system parameters	Parameter values/Equations	Source
Total alkalinity (TA) / mM	2.333	CE12010 45-CTD12
Background pCO_2*/ µatm	434	CE12010 44-HydroC; https://doi.pangaea.de/10.1594/PANGAEA.899480
Background DIC (DIC0)/ mmol kg^{-1}	2.115	Calculated from TA& pCO_2*
Background pH*	8.0	Calculated from TA& pCO_2*
Seawater temperature/ ˚C	7.8	CE12010 45-CTD12; https://doi.pangaea.de/10.1594/PANGAEA.823042
Seawater salinity/ PSU	35.18	CE12010 45-CTD12; https://doi.pangaea.de/10.1594/PANGAEA.823042
Water depth/ m	81.8	CE12010 44-ROV
Total sulfide/ mM	0	
Total boron/ mM	0.42	
Dissolved Ca ions/ mM	11.4	
Spatial DIC heterogeneity/ µM	16 or 0.7 g/m^3 excess CO_2	DIC bottom water concentrations in Tommeliten seepage area
Seasonal DIC variability/ µM	60 or 2.64 g/m^3 excess CO_2	Variability based on upper DIC bound given in Bozec et al. (2006) and lower bound measured in the Sleipner area (DIC0)
[a]Conversion of excess DIC (µM) in pCO_2 (µatm)	$pCO_2 = 1/(1 + e^{DIC_{ex} - 50}) \cdot (430 + 4 \cdot DIC_{ex} - 0.03 \cdot DIC_{ex}^2)$ $+ 1/(1 + e^{50 - DIC_{ex}}) \cdot (480 + 2.1 \cdot DIC_{ex} + 0.03 \cdot DIC_{ex}^2 - 0.00016 \cdot DIC_{ex}^3)$	Fit to model-derived data (valid up to DIC_{ex} of 1000 µM)

Details on the accuracy of data fits and the correlation of fit parameters are provided in the supplementary material.

Schmidt number Sc_T:

$$D_T = \frac{v_T}{Sc_T} \left[\frac{m^2}{s} \right] \tag{7}$$

Where Sc_T is a model constant with a typical value of 0.71 (Gualtieri et al., 2017), and v_T is calculated numerically based on the turbulent kinetic energy (k in $m^2\,s^{-2}$) and the dissipation rate of turbulent kinetic energy (ε in $m^2\,s^{-3}$) determined by the k-ε turbulence model:

$$v_T = c_\mu \frac{k^2}{\varepsilon} \left[\frac{m^2}{s} \right] \tag{8}$$

where $c\mu$ is a dimensionless model constant (i.e. 0.09; Launder and Spalding, 1974). Using the k-ε turbulence model, turbulent velocities (u), viscosities (v_T) and diffusivities (D_T) are calculated numerically, based on a transfer function of the measured current velocity magnitude (i.e. least- squares fit to the velocity data at 3.2 masf during OCE2) and algebraically specified mixing length (L_T) and turbulent intensity (I_T) defined as inlet boundary condition (Table 2). By defining an equivalent sand roughness height (k_{seq}) of 3.2 μm at the seafloor, which is related to the roughness length (z_0) by $z_0 = k_{seq}/30$ (Lefebvre et al., 2011), the non-slip boundary condition at the bottom of the model domain accounts for friction at the seabed and the resulting decline in average flow velocity towards the seabed.

The spread of dissolved CO_2 during the experiment was obtained from coupling the physics interface of mass transport (tds) to the k-ε turbulence model (i.e. the spf physics interface), thus, accounting for modifications in the advective and diffusive phenomena that the obstacle of the Ocean Elevator induced.

To significantly lower the computational requirements when solving for the turbulent flow and mass transport during the tidal turn (e.g. avoiding too many open boundaries that are weakly constrained), the effect of the tidal currents passing the Ocean Elevator geometry was simulated by rotating the obstacle in the model domain relative to a constant flow direction (defined as normal velocity condition at the inlet boundary). The outflow boundary in streamline direction is set as a zero-gradient condition, which accounts for advective mass transfer but neglects any diffusive fluxes across the boundary. The remaining boundaries are defined as slip, no-flow boundary conditions with no-friction, no-viscous forces, and no-mass transfer for seawater or dissolved species. The angles between the current flow and the Ocean Elevator during the tidal turn were calculated by correlating UTC time stamps of ADCP data (i.e. resultant current direction), and ROV position and heading during pCO_2 measurements. Based on the spatial orientation of the Ocean Elevator, whose long side was heading 40° to the north-east, two rotation angles of 40° and 70° were determined, in which most of the HydroC-pCO_2 measurements occurred and for which the simulations were run.

Initial DIC concentrations and current velocities in the model domain are prescribed to be zero, so that the model calculates excess DIC concentration relative to the background signal observed in the field (Table 4). After proving sufficient model stability by mass balance error calculations, model results were evaluated against averaged pCO_2 measurements (Fig. 5B) in order to fit the turbulent parameters (turbulent length scale and turbulent intensity) and validate the model for further application of the leaky well scenarios.

2.5. Simulating CO_2 leakage from a well

The second modelling case is designed to simulate a range of hypothetic, but realistic scenarios of CO_2 release along an abandoned well from the Sleipner CO_2 storage site into the North Sea, using site-specific current velocity data (Fig. 6) as well as initial bubble sizes (Fig. 4A) and gas flows found at methane-leaking wells in the vicinity (Vielstädte et al., 2015). The computational domain is set to be $600 \times 600 \times 20\,m^3$ with the point-source ($\sim 4\,m^2$) CO_2 leak located at the seafloor in the model center. The non-uniform mesh has a spatial resolution of

0.15–3 m with a higher finite element density about 80 m around the gas release spot.

Based on gas emissions measured at methane-leaking wells (Vielstädte et al., 2015), we define possible leakage rates (R_{CO2}) of 10, 20, and $55\,t\,yr^{-1}$ of CO_2. The advective flow (u) is prescribed from least-squares fits to 12-h time-series data of current velocities in east (x) and north (y) directions (OCE1 Bin1) considering the velocity decrease towards the seabed induced by friction (Eq. (5), Table 3).

The chosen 12-h time-series data was found to be representative for a whole tidal cycle because the North Sea has a semi-diurnal tide (Fig. 6A). The model accounts for friction at the seabed, so that the advective flow and the turbulent diffusivity are assumed to be horizontally, but not vertically and temporally uniform.

Four open lateral boundaries with a zero-gradient boundary condition allow for convective flow in and out of the model domain, while any diffusive fluxes are neglected. The lower and upper boundaries at the seafloor and towards the sea surface are set to no-flow conditions, i.e. no-mass transfer permitted; no gas exchange with the atmosphere considered. Initial DIC concentrations and current velocities in the model domain are prescribed to be zero, so that the model calculates excess DIC concentration relative to the background signal observed in the field. To ensure mass balance, the computational domain is tested to be sufficiently large to avoid that plumes of dissolved CO_2 leaving the model domain may return through the boundaries within the simulated time span.

3. Results and discussions

3.1. The gas release experiment

ROV video observation revealed moderate gas bubbling on top of the Ocean Elevator (Fig. 2). In total, 18 single CO_2 bubble streams with initial bubble sizes of 1.3 to 2.9 mm in radius (Fig. 4A) were emanating from the release head and reached a final rise height of $\sim 2\,m$. This is consistent with pCO_2 measurements which did not exceed the local background value (~ 430 μatm) two meters above the release spot (Fig. 3C).

Rapid CO_2 bubble dissolution into seawater significantly increased the bottom water partial pressure of CO_2 close to the release site to values of 2327 μatm (3 m downstream of the release, Fig. 3C). However, elevated pCO_2 levels were only observed in a very narrow band ($< 1\,m$ width) of water mass downstream of the Ocean Elevator. As a result of quick dispersion by ambient bottom currents, background values were attained already $\sim 30\,m$ downstream of the artificial leak, indicating that the impact of the experiment was limited to near-bottom waters and a rather small distance of a few tens of meters downstream of the leak (Fig. 3). This observation is in line with the QICS CO_2 injection experiment, where the CO_2 concentration away from the injection site was undetectably small and the detectable signal was confined to a small area in the vicinity of the injection point (Mori et al., 2015; Blackford et al., 2014).

Although the experiment successfully simulated CO_2 leakage into the North Sea at low rates, the physical response in the dynamic water column was quite complex. The numerical model successfully simulated the suppressed pressure and advective flow downstream of the Ocean Elevator, which induced a downwelling of the solute CO_2 plume (Fig. 5A). This effect was particularly strong at the beginning of the experiment, when the turbulent flow was heading towards the long side of the Ocean Elevator (Figs. 3A, 5A). During our experiment the density increase of water masses caused by CO_2 dissolution has no considerable effect on the observed down-welling because the maximum pCO_2 value recorded induces an increase in seawater density of $< 0.001\,kg\,m^{-3}$ (Duan et al., 1992, 2006). However, for larger leakage rates the density effect will become more important.

According to numerical results, the turbulent diffusion coefficient varied in the order of 10^{-4} to $10^{-7}\,m^2\,s^{-1}$ during the experiment. Low
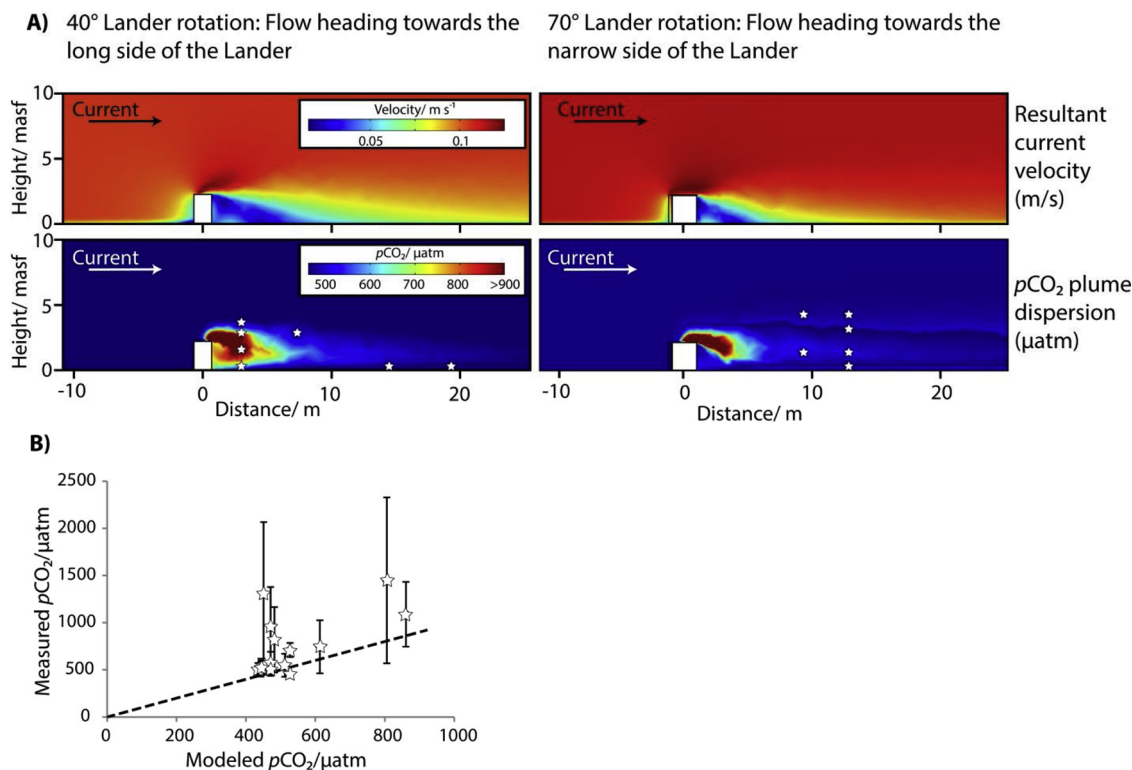
Fig. 5. A) COMSOL model results of the GRE simulation showing the modified current velocity field (top) and the dispersion of the solute CO_2 plume (bottom) downstream of the Ocean Elevator/Lander (white box) for the two simulated rotation angles of the Lander relative to a normal flow vector (black and white arrow). B) Comparison of pCO_2 measurements and model-derived pCO_2 values for each ROV measuring position (white stars) indicating that the COMSOL model under-estimates measured values but is in the scatter of most measurements. Model-derived pCO_2 values bear an uncertainty of ± 124.5 µatm as determined from the standard deviation (1σ) of the least-squares data fit that was used in the model to convert DIC concentrations into pCO_2 data (see Table 4). The 1:1 line of model-derived pCO_2 values and HydroC-pCO_2 measurements is indicated by the dashed line.

turbulent diffusivities occurred close to the seafloor and downstream of the Ocean Elevator in the region of slow advective flow (Fig. 5A). Thus, it is evident that the experimental setup not only significantly decreased the horizontal advective transport, but also suppressed the turbulent

mixing of the CO_2 plume downstream of the Ocean Elevator.

Evaluation of the numerical results against pCO_2 measurements reveals that the applied numerical models accurately describe the rapid CO_2 bubble dissolution in seawater and the spatial and temporal
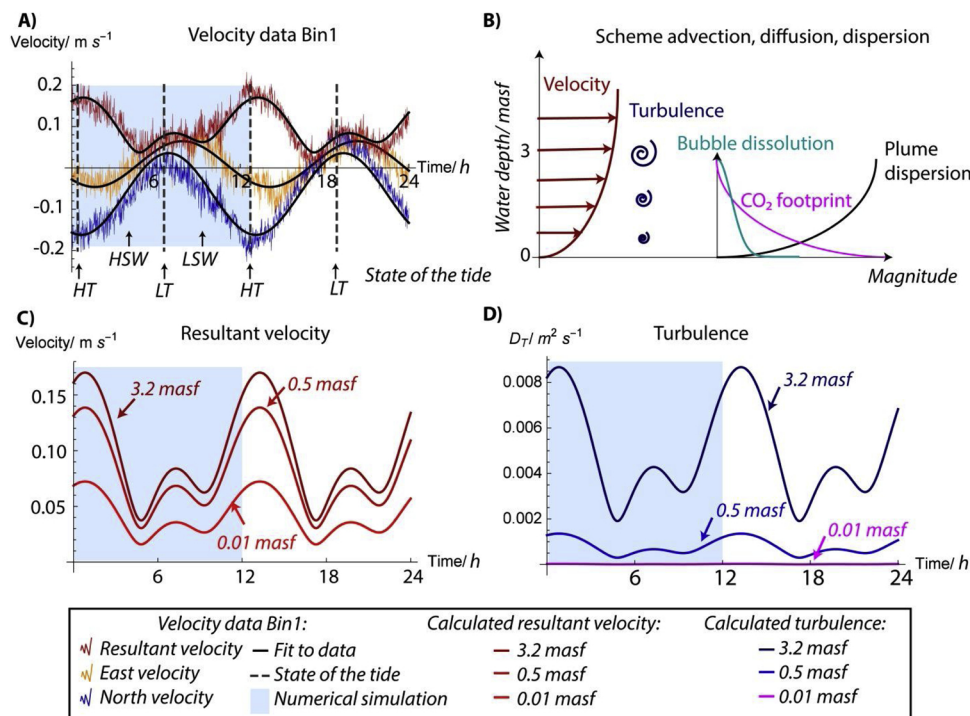

Fig. 6. A) ADCP velocity data in north (blue), east (orange), and resultant (red) current direction measured 3.2 m above the seafloor during the OCE1 long-term deployment of the ADCP. Data show a tidal asymmetry, referring to differences in the ebb and flood current velocities, i.e. stronger currents during high tide (HT) than during low tide (LT) and weaker currents during high slack water (HSW) than during low slack water (LSW). B) Scheme illustrating the Law of the Wall (LOW), where the current flow (dark red) and turbulence (dark blue) increase with distance to the seafloor, which results in the weakest dispersion of the CO_2 plume at the seafloor. Together with the declining rate of CO_2 dissolution during bubble ascent, this causes the largest CO_2 footprints (pink line) to occur at the seabed. Figures C) and D) show current velocities and turbulent diffusivities, respectively, calculated by application of the LOW in the lower 3.2 m of the water column. The first 12 h of the velocity/turbulence data set were employed for the leaky well scenarios (area shaded in light blue).

dynamics of excess CO_2 in a tidal flow (Figs. 4B, 5 A). *In situ* measurements of the spatial pCO_2 dispersion correspond well to numerical simulations, showing that bubbles are depleted in CO_2 1.9 m above their release (Fig. 4B) and the added CO_2 is diluted quickly in ambient bottom waters (Fig. 5A). Nonetheless, the model tends to underestimate pCO_2 values measured in the field as the modeled values cluster in the lower range of the pCO_2 measurements (Fig. 5B). Possible explanations for this deviation are 1) short-term fluctuations in the real advective flow, which have not been considered in the model, 2) the influence of the ROV and its thrusters on the current flow, also not considered in the model, and 3) numerical diffusivity introduced to the model.

One simplification in the model is that the advective flow acts in the direction of the Reynolds-averaged velocity and not in the real instantaneous direction of the current velocity in the field, where abrupt changes in the flow direction might have resulted in patches of high pCO_2 waters that separated from the main plume, and thus, shortly increased pCO_2 signals measured in the field. The effect of short-term fluctuations is consistent with the large scatter ($\pm$ 25% on average) in pCO_2 measurements for each measuring position (Fig. 5B). Furthermore, as the HydroC-pCO_2 sensor was attached to the front porch of the ROV, pCO_2 measurements were likely influenced by the obstacle when the plume hits the ROV (similar to the effect of the Ocean Elevator). Unphysical, numerical diffusivity, which would also result in an underestimation of measured pCO_2 values, has been minimized by tuning the lower concentration gradient limit (g_{lim}) for artificial diffusion, but may have influenced our simulations.

Despite these simplifications described above, the model captures the main features of the data; i.e. rapid bubble dissolution, quick dispersion, narrow width of the plume, and the downwelling of the plume leeward of the obstacle. We therefore argue that the applied models are sufficiently reliable to predict solute plume dispersion in the near field of a small CO_2 leak. Nonetheless, it should be noted that limitations to our modelling are related to bubble plumes and gas bubbles coated with surfactants, which physics have not been considered in our numerical simulations.

3.2. The leaky well scenarios

The simulated leaky well scenarios (Fig. 6) with constant and continuous CO_2 leakage of 10, 20 and 55 t yr^{-1}, respectively, resulted in dynamic plumes of acidified bottom water that were quickly dispersed from the source location. Generally, within a distance of less than 120 m from the leak, background pCO_2 levels are predicted (Fig. 7A). As expected, the magnitude of seawater acidification and the spatial extent of detectable CO_2 plumes at the seafloor increased with increasing leakage rates. The strongest acidification was found for the high emission scenario (55 t yr^{-1}) at high slack water (HSW) when the bottom water pH value dropped significantly from a background of 8.0 to less than 6.0. (Fig. 7C).

The simulated initial bubble size distribution with a peak radius of 2.6 mm (Vielstädte et al., 2015) loses its CO_2 almost completely within the lower 2 m of the water column. 80% of its initial CO_2 content is already dissolved within the first meter above the seafloor (Fig. 4B). Such rapid CO_2 bubble dissolution causes leaking CO_2 to remain in the bottom waters and inhibits direct bubble transport into the atmosphere. This is in line with our experimental results and other recent studies (Hvidevold et al., 2015; Dewar et al., 2013; Dissanayake et al., 2012; Phelps et al., 2014; Kano et al., 2010). However, once a leak occurs, some of the dissolved CO_2 may ultimately reach the atmosphere via diffusive sea-air gas exchange, mostly depending on the mixing of the water column and the water depth at which leakage were to occur (Phelps et al., 2014).

In the following, we discuss key drivers controlling the dispersion of CO_2 emitted at a point source in a tidally influenced oceanic setting (section 3.2.1), before discussing modelling-derived estimates on the spatial footprints of potentially harmful and detectable CO_2 plumes in

seawater in order to support risk assessments (section 3.2.2) and monitoring strategies (section 3.2.3) of offshore CO_2 storage sites, respectively. Finally, we discuss the propensity of wells to leak at Sleipner (section 3.2.4).

3.2.1. CO2 plume dispersion and relationship with tides

Using the tidal velocity data of July 12th 2012 for the CNS (Fig. 6A), our leaky well simulations show a strong correlation between the dispersion of the dissolved CO_2 plume in the water column and the phase of the semi-diurnal tides (Fig. 7). Common temporal and spatial features include (1) the accumulation of DIC near the leak during periods of decelerating flow, (2) thin elongated plumes with low DIC concentrations during periods of strong unidirectional flow, (3) wider plume shapes when the tides turn, and (4) extensive build-up of DIC peak concentrations during slack water periods with low or stagnant flow (which is in line with other recent studies, e.g. Greenwood et al., 2015, Fig. 7A).

These observations indicate that continuous CO_2 leakage into the North Sea would result in a series of plume concentrations and shapes during a tidal cycle, with peak concentrations and largest plume footprints occurring around slack water periods and close to the seafloor, where advective and diffusive fluxes are low (Fig. 6). In contrast, at stronger flow DIC concentrations should be efficiently diluted with ambient seawater quickly reaching background values.

Higher simulated DIC concentrations during low tide (*LT*) as compared to high tide (*HT*) were primarily a consequence of the measured tidal asymmetry, referring to differences in the ebb and flood current velocities (Figs. 6A, 7 C). Tides may not only affect CO_2 dispersion but also the CO_2 emission rate at the seabed since studies at natural gas seeps (e.g. Leifer and Wilson, 2007; Linke et al., 2010; Tryon et al., 1999; Wiggins et al., 2015) and the QICS CO_2 injection experiment (Blackford et al., 2014) imply that rates of bubble release at the seafloor respond to tidal pressure fluctuations.

Calculated turbulent diffusion coefficients (D_T) were in agreement to those measured in the benthic boundary layer of permeable sediments in the Central North Sea (McGinnis et al., 2014), suggesting that the applied correlation of D_T and measured current velocities (Eq. (6)) yielded realistic results. In our simulations, D_T at 3.2 m above the seabed varied between $2 \cdot 10^{-3}$ m^2 s^{-1} at minimum and $9 \cdot 10^{-3}$ m^2 s^{-1} at maximum current flow velocity. It was significantly smaller, that is on the order of 10^{-7} m^2 s^{-1}, close to the seafloor (0.01 masf) throughout the whole tidal cycle (Fig. 6D). Despite the wide range of diffusion coefficients, the dimensionless Péclet number (Pe), that is the ratio of the rate of tracer advection to the rate of tracer diffusion, was always larger than 10 - an indication that diffusive fluxes were overall negligible. This implies that for a North Sea setting and at small scales lateral diffusive fluxes are low and thus, have only a negligible effect on the dispersion of the dissolved CO_2 plume, whereas the advective transport (i.e. tidal current) is a key parameter. It should however be noted, that diffusion was the only mechanism that controlled the vertical dispersion of the CO_2 plume in our three leaky well simulations, as we neglected any vertical advective transport.

3.2.2. Environmental impact of a CO2-leaking well in the CNS

The environmental impact of CO_2 leakage into seawater is a critical issue in risk assessment studies and depends on the magnitude of seawater acidification and the spatial and temporal extent of any potentially harmful pH reductions exceeding a site-specific natural variability, which marine biota should be adapted to. In the deeper layers of the Northern and Central North Sea marine DIC concentration varying between 2.11 and 2.17 mmol kg^{-1} have been observed (Bozec et al., 2006). This corresponds to a seasonal variability in pH of 7.85–8.02, assuming a constant TA of 2.333 meq. dm^{-3} (a simplification due to lacking literature data on seasonal variations in TA in North Sea bottom waters) and physicochemical seawater conditions as measured in the Sleipner area in July 2012 (T = 7.8 °C; S = 35.18, P = 9.2 bar;
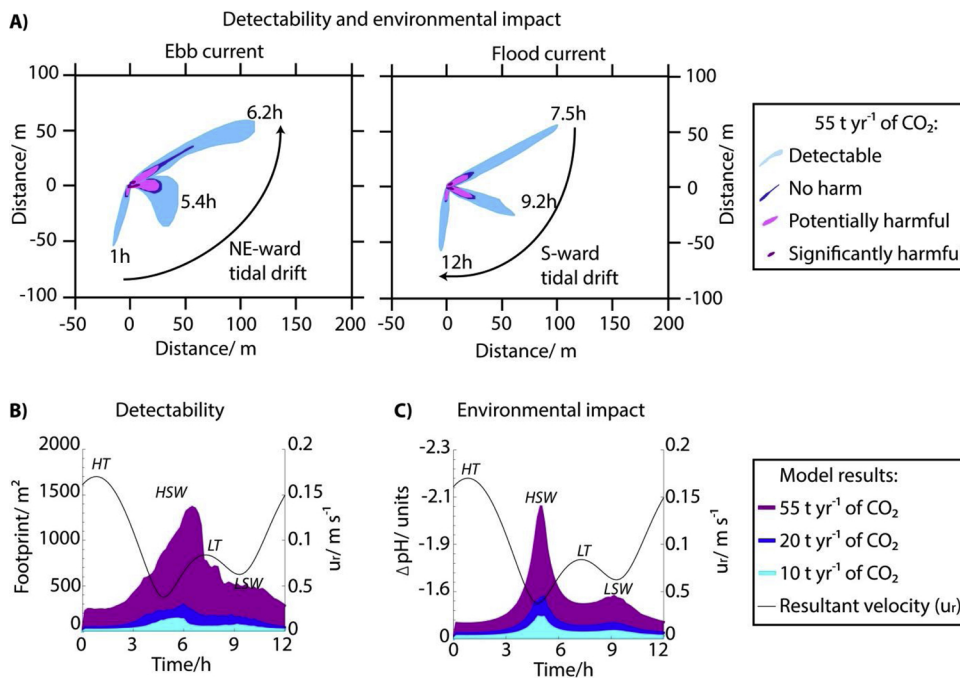
Fig. 7. A) Model-derived CO_2 plume dispersion during half a tidal cycle (12 h) showing the varying footprints of detectable (light blue) and environmentally harmful (light and dark magenta) CO_2 plumes at the seafloor. Because the threshold value for leak detection (16 μM of excess DIC) is lower than the seasonal DIC variability (60 μM, dark blue), which marine biota should be adapted to, detectable CO_2 plumes are larger than the environmentally impacted seafloor area. B) Simulated footprints of detectable CO_2 plumes and C) maximum seawater acidification at the seafloor as a function of time resulting from a leaky well in the CNS that emits 10 (cyan), 20 (blue), and 55 (magenta) t yr^{-1} of CO_2 into the water column.

Table 5

Maximum predicted seafloor areas (m^2), which are considered to be detectable ($\Delta DIC > 16$ μM), have significantly harmful impact ($\Delta pH > 1$ unit), potentially harmful impact ($0.5 > \Delta pH > 0.2$ unit), and no impact ($0.2 > \Delta pH > 0.15$ unit) on marine biota.

Leakage rate/ t yr^{-1} of CO_2	Area with significantly harmful impact ($\Delta pH > 1$ unit) / m^2	Area with potentially harmful impact ($0.5 > \Delta pH > 0.2$ unit) / m^2	Area with no deleterious impact ($0.2 > \Delta pH > 0.15$ unit) / m^2	Total impacted seafloor area ($\Delta pH > 0.15$ unit)/ m^2	Detectable seafloor footprint/ m^2
10	≤1.6	≤13.3	≤8	≤29	≤136
20	≤5	≤25	≤14	≤54	≤292
55	≤27	≤133.8	≤66	≤271	≤1364

Table 4). As such, effects of CO_2 leakage resulting in pH changes of less than -0.15 units are considered to be indistinguishable from seasonal variability (in line with other North Sea studies; e.g. Phelps et al., 2014), and thus, would have no deleterious consequences at Sleipner. Hence, to examine the extent to which marine biota might be affected by a well leaking CO_2, we refer to the seafloor area impacted by pH changes exceeding those of seasonal variability (60 μM DIC corresponding to 0.15 pH units, Fig. 7, Table 5).

Across all three leakage scenarios, the seafloor area impacted by pH changes exceeding those of seasonal variability increased with increasing leakage rate, but was always below 271 m^2 (Table 5). This indicates that the impact of a well leaking CO_2 would be extremely localized not exceeding a distance of ~80 m from the leak (Fig. 7A at LT, 7.5 h). Note, that the threshold value for leak detection (16 μM of excess DIC) is lower than the seasonal DIC variability (60 μM, dark blue), which marine biota should be adapted to, so that detectable CO_2 plumes are larger (i.e. < 1400 m^2) than the environmentally relevant impacted seafloor area (Fig. 7B). The largest simulated reduction of seawater pH occurred in bottom waters in the direct vicinity of the leak and during high slack water (HSW), where the advective and diffusive fluxes were weakest (Fig. 7C). Here, the change in pH was as high as -1.23, -1.54, and -2.10 units for the low, mid and high leakage rate, respectively. To put these values into context to the potential impact to marine biota, we follow the classification suggested by Phelps et al. (2014) and Widdicombe et al. (2013). According to these authors and results from the EU-FP7 project ECO2 (Haeckel and Blackford, 2014), long-term reductions of pH approaching or exceeding 1.0 unit can be considered as significantly harmful (i.e. significantly increasing mortality of fauna), whereas a reduction on the order of 0.2-0.5 is

potentially harmful (i.e. changing the benthic community structure). Based on this, our three leaky well scenarios indicate that CO_2 leakage, even at the smallest rate (10 t yr^{-1}), would reduce the pH below the critical value that would have a significant negative impact on benthic organisms. However, such harmful conditions would be extremely localized, occurring only in the immediate vicinity of the leak, whereas most of the impacted seafloor area would be exposed to seawater pH conditions that are considered to be potentially harmful (mid and high leakage scenario) or are unlikely to have any impact at all (low leakage scenario) (Table 5). It should be noted further that these classifications are based on experimental data, where marine organisms have been continuously exposed to reduced pH values for a couple of weeks (Widdicombe et al., 2013). Marine biota may respond differently to the transient exposures observed in our experiment and numerical simulations (Fig. 8), which is consistent with numerical computations of Kano et al. (2010). Repeated short-term (minutes to hours) exposures to low-pH waters might be less harmful than continuous exposure, suggesting that more research is necessary to examine the effect of oscillating pH changes on marine organisms.

3.2.3. Detectability and monitoring of a leaky well

Conventionally leaky wells are determined by an assessment of well integrity, generally identified by sustained casing pressure (Brufatto et al., 2003). However, this approach is unable to detect gas leakage along the outside of wells, where injected CO_2 might escape from the storage reservoir through disturbed and fractured sediments in the surrounding of the wellbore. As such, we recommend to enhance the monitoring strategy in order to detect a leaky well by correlating the well paths of boreholes poking through the storage formation with the
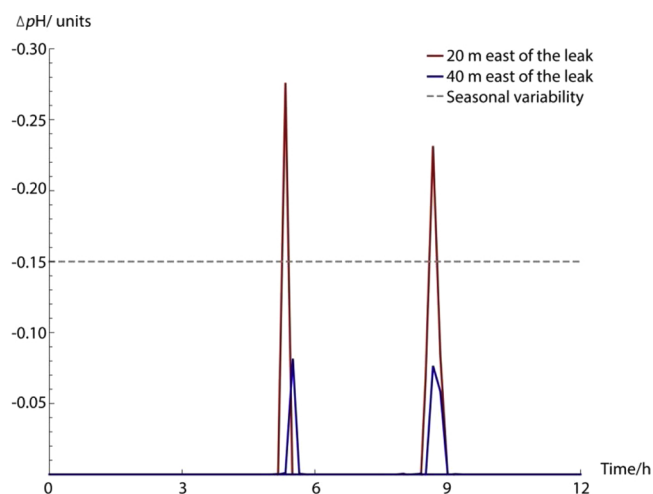
Fig. 8. Modelled seawater acidification showing the short time exposure of benthic organisms to low pH conditions 20 m (red) and 40 m (blue) east of a leaky well (20 t yr^{-1}). pH reductions exceeding those of natural variability (dashed line) are restricted to the direct vicinity of the well and occur twice in a 12 h period.

sub-seafloor location of the CO_2 plume as identified in seismic data (Vielstädte et al., 2017). Wells that were proven to penetrate the sub-surface plume or are located in its direct vicinity while also reaching the depth of the storage formation will pose a higher risk for leakage and will thus require monitoring. The survey area needs to be adjusted continuously as injection proceeds and the CO_2 plume spreads in the subsurface.

The size of the seafloor area around a "risky well" that would require monitoring is site-specific and will mostly depend on the spatial extent of the CO_2 plume in the water column, which can be geochemically distinguished from any natural variability in the carbonate chemistry. Therefore, a combination of a thorough baseline study of environmental conditions (i.e. carbonate chemistry, currents), resolving changes over relatively short time scales, and numerical modelling will enable reliable prediction of the spatial and temporal characteristics of the solute CO_2 plume in the water column. Due to the presumably small emission rates associated to a leaky well, models will need to provide a high spatial resolution to resolve the small footprint of the solute CO_2 plume in seawater.

For monitoring purposes, spatial heterogeneities, caused by short-term fluctuations in background marine DIC concentration, are more relevant than the larger seasonal variability. Nonetheless, long-term baseline studies are needed in order to obtain trends in short-term variations. In the Sleipner case, spatial heterogeneity is assumed to be on the order of 16 μM as determined by DIC measurements along a transect in the Tommeliten seepage area (supplementary material). Due to the similar water depth and physicochemical seawater conditions, a threshold of 16 μM of DIC for detecting leakage was assumed to be also representative for Sleipner. Based on this threshold value, our numerical results suggest that water column monitoring should be performed in a narrow area of less than 1400 m^2 around a "risky well" to detect leakage (Table 5). Hence, geochemical monitoring surveys need to be performed at a very high spatial resolution to capture leaking wells. Moreover, instruments (pCO$_2$ or pH sensors) should be deployed < 2 m above the seafloor to reliably detect CO_2 leakage since rapid CO_2 bubble dissolution limits detectable concentration anomalies to bottom waters in close contact with the seabed. This is in line with the final conclusions of the QICS CO_2 injection experiment, where rapid dissolution of the CO_2 bubble plume into sea water was found to significantly increase bottom-water CO_2 partial pressure close to the injection site (Blackford et al., 2014; Dewar et al., 2015).

As natural, spatial heterogeneity in the carbonate chemistry at

Sleipner (i.e. ± 16 μM of DIC, corresponding to ± 45 μatm of pCO$_2$, and ± 0.04 pH units) appears to be larger than the accuracy of most available sensors (i.e. ± 1 μmol kg^{-1} of DIC, Dickson et al., 2007, ± 30 μatm of pCO$_2$ at sensor calibration up to 3000 μatm, Fietzek et al., 2014, and ± 0.005 pH units, Shitashima et al., 2013), the probability for detecting a leaky well tends to be rather independent from the sensors applied but will likely increase with the number of *in situ* instruments available (Hvidevold et al., 2015) and the time period of continuous *in situ* monitoring. Due to a lack of temporal coverage and low spatial resolution distinct water sampling of DIC appears insufficient to capture CO_2 leakage, while continuous *in situ* monitoring over a few tidal cycles (days to weeks) is promising, which is in agreement with the final conclusions of the QICS CO_2 injection experiment (Atamanchuk et al., 2015). Finally, once a leak has been identified, long-term investigations of the environmental consequences will be necessary because fixing such leaks will be challenging.

3.2.4. Propensity of wells to leak at Sleipner

In contrast to the conventional approach of assessing the risk of wells to leak by well integrity, we evaluate the risk of CO_2 leakage along the outside of wells, currently not considered in regulatory frameworks such as the EU CCS Directive GD1 (2011) and the OSPAR Convention (2007). The larger Sleipner area hosts 80 wells, of which 39 belong to the Sleipner A platform from which CO_2 is being injected into the ~900 m deep Utsira sandstone formation (Fig. 1B). According to the 3-D seismic time-lapse data of 2008, none of these surrounding wells penetrates the subsurface plume of injected CO_2 yet (Fig. 1B) and thus, currently constitutes a risk for CO_2 leakage from the storage unit. The closest well 15/9-13, which is located around 500 m to the west of the CO_2 injection point, was ~350 m away from the outer rim of the 2008 subsurface plume and has been identified to emit shallow (~600 mbsf), biogenic methane (Vielstädte et al., 2015). Despite its vicinity to the subsurface CO_2 plume and its demonstrated gas leakage, the slow and predominantly north-eastward migration of the injected CO_2 in the storage reservoir (Eiken et al., 2011) may prevent that well 15/9-13 will pose a future risk for CO_2 leakage (Fig. 1B). However, newer time-lapse data and more sophisticated models evaluating the spreading of injected CO_2 in the storage reservoir are needed to assess if and when the injected CO_2 might reach well 15/9-13. Due to the large distance of the other wells (> 1.5 km) and the expected slow spread of the injected CO_2 in the storage reservoir (Eiken et al., 2011; Chadwick et al., 2009; Karstens et al., 2017), it is unlikely that the Sleipner CO_2 plume will reach wells other than 15/9-13 during the operation's lifetime (i.e. 30 years).

From a climate control point of view, a single leaky well with CO_2 emission rates of < 55 t yr^{-1} has insignificant impact on storage performance. In the Sleipner case, CO_2 injection at 1 Mt yr^{-1} and leakage of 55 t yr^{-1} would mean losses of 0.006% per year, which falls below the 0.01% per year, being considered as a threshold value to retain the long-term (millennium) suitability of CCS as a climate change mitigation option (Haugan and Joos, 2004). Considering the long-term suitability of CCS and CDR is important because leakage along a well (similar to natural conduits, such as faults and fractures) may persist for a long time, far beyond the active period of CO_2 injection, due to the slow dissolution of the injected CO_2 in the formation waters, the buoyancy-driven leakage, and the challenge to fix such leaks. At Sleipner, reservoir simulations have indicated that the injected CO_2 will completely dissolve within around 4000 years (Torp and Gale, 2004), determining the timespan for which the fugitive loss of CO_2 could theoretically continue. However, CO_2 dissolution and the associated loss of buoyancy starts immediately after injection and may become efficient in shorter timespans (i.e. around 500-1000 years), thereby reducing the amount of CO_2 that could be lost from the reservoir (Kempka et al., 2014). As such, only prolonged leakage along numerous wells would create a sustained non-tolerable leakage rate above 0.01% at Sleipner. Our study stresses the importance of leak detection and emphasizes that the

conventional focus on well integrity needs to be extended because it neglects the potential escape of injected CO_2 through drilling-induced fractures along the outside of wells. From this perspective developed hydrocarbon provinces with high well density may not always be the most suitable areas for CO_2 storage.

4. Conclusions

This study presents the results of a field experiment in the North Sea simulating the leakage of CO_2 through abandoned wells. The chosen release rate (31 t yr^{-1}) falls into the range of natural gas emissions through abandoned wells previously quantified in the area (Vielstädte et al., 2015, 2017). At the experimental leakage rate, CO_2 gas bubbles are completely dissolved within 2 m above the seabed. Hence, CO_2 is not emitted into the atmosphere but retained in the lower water column of the North Sea. Strong tidal currents and cycles, both prominent in the North Sea, significantly diminish the spread of high-CO_2 and low-pH water masses into the far field of a leak by efficiently diluting elevated CO_2 levels with background concentrations. Nonetheless, even moderate CO_2 emissions have harmful effects on benthic marine organisms living in the direct vicinity of a leaky well, especially during periods of low or stagnant current flow. These effects might be mitigated by the tidally oscillating flow that periodically restores natural pH conditions close to the leak. Monitoring of abandoned wells has to resolve the hydro-acoustic and/or chemical signals directly at the seabed since leaked CO_2 can only be detected at < 2 m above the seafloor. Moreover, it has to be performed at a small lateral distance to the well since the chemical signal can only be resolved < 100 m downstream of the well. Finally, it is important to consider the tidal nature of the current regime and provide chemical measurements during a tidal period where the sampling point is downstream of the considered well. Prolonged leakage along numerous well paths may compromise the long-term performance of a CO_2 storage complex. Hence, the conventional focus on well integrity needs to be extended because it neglects the potential escape of injected CO_2 through drilling-induced fractures along the outside of abandoned wells.

Authors contributions

The paper was written by L.V., supervised by M.H., and K.W. The gas release experiment was designed by P.L., S.S., and M.S. Geochemical and optical data were collected and analyzed by P.L., M.S., M.H., S.S., and L.V. Numerical modelling and data evaluation were done by L.V and M.B.

Author information

The authors declare no competing financial interests. Correspondence and requests for materials should be addressed to K.W. (kwallmann@geomar.de) and M.H. (mhaeckel@geomar.de).

Acknowledgments

Appendix A. Supplementary data

Supplementary material related to this article can be found, in the online version, at doi:https://doi.org/10.1016/j.ijggc.2019.03.012. Raw data of ADCP, CTD, and HydroC-pCO$_2$ measurements can be downloaded from the World Data Center PANGAEA, at https://doi.pangaea.de/10.1594/PANGAEA.833751, https://doi.pangaea.de/10.1594/PANGAEA.833761, https://doi.pangaea.de/10.1594/PANGAEA.823042, https://doi.pangaea.de/10.1594/PANGAEA.899480. Supplementary video data of our gas release experiment can be downloaded from the link: https://www.pangaea.de/tok/e3a4d8996affba87b666c04d969672657c32313d.

References

Arts, R., Chadwick, A., Eiken, O., Thibeau, S., Nooner, S., 2008. Ten years' experience of monitoring CO_2 injection in the Utsira sand at Sleipner, offshore Norway. First Break 26, 65–72.

Atamanchuk, et al., 2015. Detection of CO_2 leakage from a simulated sub-seabed storage site using three different types of pCO$_2$ sensor. Int. J. Greenh. Gas Control 38, 121–134. https://doi.org/10.1016/j.ijggc.2014.10.021.

Bachu, S., Watson, T.L., 2009. Review of failures for wells used for CO_2 and acid gas injection in Alberta, Canada. Energy Procedia 1, 3531–3537. https://doi.org/10.1016/j.egypro.2009.02.146.

Blackford, J., et al., 2014. Detection and impacts of leakage from sub-seafloor deep geological carbon dioxide storage. Nat. Clim. Change 4, 1011–1016. https://doi.org/10.1038/NCLIMATE2381.

Boudreau, B.P., 1997. Diagenetic Models and Their Implementation: Modelling Transport and Reactions in Aquatic Sediments. Springer, Berlin, Heidelberg, New York, London, Paris, Tokyo, Hong Kong, pp. 414.

Bozec, Y., et al., 2006. Assessment of the processes controlling seasonal variations of dissolved inorganic carbon in the North Sea. Limnol. Oceanogr. 51 (6), 2746–2762.

Brufatto, C., et al., 2003. From mud to cement - Building gas wells. Oilfield Rev. 15, 62–76.

Carey, J.W., et al., 2007. Analysis and performance of oil well cement with 30 years of CO_2 exposure from the SACROC Unit, West Texas, USA. Int. J. Greenh. Gas Control 1, 75–85.

Carey, J.W., Svec, R., Grigg, R., Zhang, J., Crow, W., 2010. Experimental investigation of wellbore integrity and CO_2-brine flow along the casing-cement microannulus. Int. J. Greenh. Gas Control 4, 272–282.

Chadwick, R.A., Noy, D., Arts, R.J., Eiken, O., 2009. Latest time-lapse seismic data from Sleipner yield new insights into CO_2 plume development. Energy Procedia 1, 2103–2110. https://doi.org/10.1016/j.egypro.2009.01.274.

Codina, R., 1998. Comparison of some finite element methods for solving the diffusion-convection-reaction equation. Comput. Methods Appl. Mech. Eng. 156, 185–210.

Crow, W.J., Carey, J.W., Gasda, S.E., Williams, D.B., Celia, M., 2010. Wellbore integrity analysis of a natural CO2 producer. Int. J. Greenh. Gas Control 4 (2), 186–197.

Dewar, M., Wei, W., McNeil, D., Chen, B., 2013. Small-scale modelling of the physico-chemical impacts of CO_2 leaked from sub-seabed reservoirs or pipelines within the North Sea and surrounding waters. Mar. Pollut. Bull. 73 (August(2)), 504–515.

Dewar, M., Sellami, N., Chen, B., 2015. Dynamics of rising CO_2 bubble plumes in the QICS field experiment Part 2- Modelling. Int. J. Greenh. Gas Control 38, 52–63.

Dickson, A., Sabine, C., Christian, J.E., 2007. Guide to best practices for ocean CO_2 measurements. PICES Spec. Publ. 3.

Dissanayake, A.L., et al., 2012. Modeling the impact of CO_2 releases in Kagoshima Bay, Japan. J. Hydro Environ. Res. 6, 195–208.

Do Carmo, E.G., Alvarez, G.B., 2003. A new stabilized finite element formulation for scalar convection-diffusion problems. Comput. Methods Appl. Mech. Engrg. https://doi.org/10.1016/S0045-7825(03)00292-5.

Duan, Z., MØller, N., Weare, J.H., 1992. An equation of state for the CH$_4$-CO$_2$-H$_2$O system: 1. Pure systems from 0 to 1000˚C and 0 to 8000 bar. Geochim. Cosmochim. Ac. 56 (14), 2605–2617.

Duan, Z., Sun, R., Zhu, C., Chou, I.M., 2006. An improved model for the calculation of CO_2 solubility in aqueous solutions containing Na$^+$, K$^+$, Ca^{2+}, Mg^{2+}, CL$^-$, and SO$_4^{2-}$. Mar. Chem. 98, 131–139.

Eiken, O., et al., 2011. Lessons Learned from 14 years of CCS Operations: Sleipner, In Salah and SnØhvit. Energy Procedia 4, 5541–5548.

EU CCS Directive GD1, 2011. Implementation of Directive 2009/31/EC on the Geological Storage of Carbon Dioxide. Guidance Document 1, CO_2 Storage Life Cycle Risk Management Framework. pp. 60.

EU GeoCapacity, 2009. Assessing Europe Capacity for Geological Storage of Carbon Dioxide. D16 WP2 Storage Capacity. pp. 170.

Farreira, T., Rasband, W., 2012. ImageJ User Guide IJ 1.46r. pp. 185p. http://imagej.nih.gov/ij/docs/guide/index.html.

Fiedler, B., et al., 2013. In situ CO_2 and O_2 measurements on a profiling float. J. Atmos. Ocean Technol. 30, 112–126. https://doi.org/10.1175/JTECH-D-12-00043.1.

Fietzek, P., Fiedler, B., Steinhoff, T., Körtzinger, A., 2014. In situ quality assessment of a novel underwater pCO$_2$ sensor based on membrane equilibration and NDIR spectrometry. J. Atmos. Ocean Technol. 31, 181–196. https://doi.org/10.1175/JTECH-D-13-00083.1.

Gasda, S., Bachu, S., Celia, M., 2004. The potential for CO_2 leakage from storage sites in geological media: analysis of well distribution in mature sedimentary basins. Environ.

Geol. 46 (67), 707–720.

Geng, M., Duan, Z.H., 2010. Prediction of oxygen solubility in pure water and brines up to high temperatures and pressures. Geochim. Cosmochim. Ac. 74, 5631–5640.

GEOMAR Helmholtz-Zentrum für Ozeanforschung Kiel, 2017. Remotely Operated Vehicle "ROV KIEL6000". J. Large-Scale Res. Facil. 3, A117. https://doi.org/10.17815/jlsrf-3-160.

Greenwood, J., Craig, P., Hardman-Mountford, N., 2015. Coastal monitoring strategy for geochemical detection of fugitive CO_2 seeps from the seabed. Int. J. Greenh. Gas Control 39, 74–78. https://doi.org/10.1016/j.ijggc.2015.05.010.

Gualtieri, C., Angeloudis, A., Bombardelli, F., Jha, S., Stoesser, T., 2017. On the values for the turbulent schmidt number in environmental flows. Fluids 2 (17) doi:10.3390.

Gurevich, A.E., Endres, B.L., Robertson Jr., J.O., Chilingar, G.V., 1993. Gas migration from oil and gas fields and associated hazards. J. Petr. Sci. Eng 9, 233–238.

Haeckel, M., Blackford, J., 2014. CCT2 Synthesis Report on Predicted Impacts and Uncertainties, ECO2 Deliverable D12.3. pp. 42. https://doi.org/10.3289/ECO2_D12.3).

Haugan, P.M., Joos, F., 2004. Metrics to assess the mitigation of global warming by carbon capture and storage in the ocean and in geological reservoirs. Geophys. Res. Lett. 31, L18202. https://doi.org/10.1029/2004GL020295.

Hvidevold, H.K., et al., 2015. Layout of CCS monitoring infrastructure with highest probability of detecting a footprint of a CO_2 leak in a varying marine environment. Int. J. Greenh. Gas Control 37, 274–279. https://doi.org/10.1016/j.ijggc.2015.03.013.

IPCC, 2014. In: Edenhofer, O., Pichs-Madruga, R., Sokona, Y., Farahani, E., Kadner, S., Seyboth, K., Adler, A., Baum, I., Brunner, S., Eickemeier, P., Kriemann, B., Savolainen, J., Schlömer, S., von Stechow, C., Zwickel, T., Minx, J.C. (Eds.), Climate Change 2014: Mitigation of Climate Change. Contribution of Working Group III to the Fifth Assessment. Report of the Intergovernmental Panel on Climate Change. Cambridge University Press, Cambridge, United Kingdom and New York, NY, USA.

Jordan, A.B., Stauffer, P.H., Harp, D., Carey, J.W., Pawar, R.J., 2015. A response surface model to predict CO_2 and brine leakage along cemented wellbores. Int. J. Greenhous Gas Control 33, 27–39. https://doi.org/10.1016/j.ijggc.2014.12.002.

Kano, Y., Sato, T., Kita, J., Hirabayashi, S., Tabeta, S., 2010. Multi-scale modeling of CO_2 dispersion leaked from the seafloor off the Japanese coast. Mar. Pollut. Bull. 60, 215–224.

Karstens, J., Ahmed, W., Berndt, C., Class, H., 2017. Focused fluid flow and the sub-seabed storage of CO_2: evaluating the leakage potential of seismic chimney structures for the Sleipner CO_2 storage operation. Mar. Pet. Geol. 88, 81–93.

Kempka, T., De Lucia, M., Kühn, M., 2014. Geomechanical integrity verification and mineral trapping quantification for the Ketzin CO_2 storage pilot site by coupled numerical solutions. Energy Procedia 63, 3330–3338.

Kundu, P.K., Cohen, I.M., 2008. Fluid Mechanics, 4th ed. Elsevier.

Kutchko, B.G., Strazisar, B.R., Dzombak, D.A., Lowry, G.V., Thaulow, N., 2007. Degradation of wellbore cement by CO_2 under geologic sequestration conditions. Environ. Sci. Technol. 41, 4787–4792.

Launder, B.E., Spalding, D.B., 1974. The numerical computation of turbulent flows. Comput. Methods Appl. Mech. Eng. 3, 269–289.

Lefebvre, A., Ernstsen, V.B., Winter, C., 2011. Influence of compound bedforms on hydraulic roughness in a tidal environment. Ocean Dyn. 61 (12), 2201–2210.

Leifer, I., Wilson, K., 2007. The tidal influence on oil and gas emissions from an abandoned oil well: nearshore Summerland, California. Mar. Pol. Bull 54 (9), 1495–1506.

Leifer, I., et al., 2015. The fate of bubbles in a large, intense bubble megaplume for stratified and unstratified water: Numerical simulation of 22/4b Expedition field data. Mar. Petrol. Geol. 68, 806–823.

P. Linke, (Editor), RV Celtic Explorer EUROFLEETS Cruise Report CE12010 - ECO2@ NorthSea : 20.07. - 06.08.2012, doi: 10.3289/GEOMAR_REP_NS_4_2012 2012, 60 Bremerhaven - Hamburg. GEOMAR Report, N. Ser. 004. GEOMAR, Kiel, Germany.

Linke, P., Sommer, S., Rovelli, L., McGinnis, 2010. Physical limitations of dissolved methane fluxes: the role bottom-boundary layer processes. Mar. Geol. 272, 209–222. https://doi.org/10.1016/j.margeo.2009.03.020.

Linke, P., Schmidt, M., Rohleder, M., Al-Barakati, A., Al-Farawati, R., 2015. Novel online digital video and high-speed data broadcasting via standard coaxial cable onboard marine operating vessels. Mar. Technol. Soc. J. 49 (1), 7–18.

Mao, S., Duan, Z.H., 2006. A thermodynamic model for calculating nitrogen solubility, gas phase composition and density of the N_2-H_2O-NaCl-system. Fluid Phase Equilibr 248, 103–114.

McGinnis, D.F., Sommer, S., Lorke, A., Glud, R.N., Linke, P., 2014. Quantifying tidally driven benthic oxygen exchange across permeable sediments: an aquatic eddy correlation study. J. Geophys. Res. Oceans 119, 6918–6932. https://doi.org/10.1016/2014JC010303.

Metz, B., Davidson, O., De Coninck, H.C., Loos, M., 2005. IPCC Special Report on Carbon Dioxide Capture and Storage. Prepared by Working Group III of the Intergovernmental Panel on Climate Change. IPCC.

Mori, C., et al., 2015. Numerical study of the fate of CO_2 purposefully injected into the sediment and seeping from the seafloor in Ardmucknish Bay. Int. J. Greenh. Gas Control 38, 153–161.

Nordbotten, J.M., Celia, M.A., Bachu, S., Dahle, H.K., 2005. Semianalytical solution for CO_2 leakage through an abandoned Well. Environ. Sci. Technol. 39, 602–611.

OSPAR Convention, 2007. OSPAR Guidelines for Risk Assessment and Management of Storage of CO_2 Streams in Geological Formations. Reference Number 07-12. pp. 32.

Phelps, J.J.C., Blackford, J.C., Holt, J.T., Polton, J.A., 2014. Modelling large-scale CO_2 leakages in the North Sea. Int. J. Greenh. Gas Control. https://doi.org/10.1016/j.ijggc.2014.10.013.

Press, W.H., Teukolsky, S.A., Vetterling, W.T., Flannery, B.P., 2007. Numerical Recipes: The Art of Scientific Computing, third ed. Cambridge University Press, Cambridge.

Schneider von Deimling, J., Linke, P., Schmidt, M., Rehder, G., 2015. Ongoing methane discharge at well site 22/4b (North Sea) and discovery of a spiral vortex bubble plume motion. Mar. Pet. Geol. 68, 718–730.

Sellami, N., Dewar, M., Stahl, H., Chen, B., 2015. Dynamics of rising CO_2 bubble plumes in the QICS field experiment Part 1 – the experiment. Int. J. Greenh. Gas Control 38, 44–51.

Shitashima, K., Maeda, Y., Ohsumi, T., 2013. Strategies for detection and monitoring of CO_2 leakage in sub-seabed CCS. Energy Procedia 37, 4283–4290. https://doi.org/10.1016/j.egypro.2013.06.331.

Sofroniou, M., Knapp, R., 2008. Wolfram Mathematica Tutorial Collection- Advanced Numerical Differential Equation Solving in Mathematica. Wolfram Research, Inc.

Tao, Q., Bryant, S.L., 2014. Well permeability estimation and CO_2 leakage rates. Int. J. Greenh. Gas Control 22, 77–87. https://doi.org/10.1016/j.ijggc.2013.12.022.

Torp, T.A., Gale, J., 2004. Demonstrating storage of CO_2 in geological reservoirs: The Sleipner and SACS projects. Energy 29, 1361–1369.

Tryon, M.D., et al., 1999. Measurements of transience and downward fluid flow near episodic gas vents, Hydrate Ridge, Cascadia. Geology 27, 1075–1078.

UNESCO, 1981. The practical salinity scale 1978 and the international equation of state of seawater 1980. Tech. Pap. Mar. Sci 36, 25.

Vielstädte, L., Karstens, J., Haeckel, M., Schmidt, M., Linke, P., Reimann, S., Liebetrau, V., McGinnis, D.F., Wallmann, K., 2015. Quantification of methane emissions at abandoned gas wells in the Central North Sea. Mar. Petrol. Geol 68, 848–860.

Vielstädte, L., Haeckel, M., Karstens, J., Linke, P., Schmidt, M., Steinle, L., Wallmann, K., 2017. Shallow gas migration along hydrocarbon wells-An unconsidered, anthropogenic source of biogenic methane in the North Sea. Environ. Sci. Technol. 51 (17), 10262–10268. https://doi.org/10.1016/j.marpetgeo.2015.07.030.

Widdicombe, S., Blackford, J.C., Spicer, J.I., 2013. Assessing the environmental consequences of CO2 leakage from geological CCS: generating evidence to support environmental risk assessment. Mar. Pollut. Bull. 73 (2), 399–401.

Wiggins, S.M., Leifer, I., Linke, P., Hildebrand, J.A., 2015. Long-term acoustic monitoring at North Sea well site 22/4b. Mar. Petrol. Geol 68, 776–788. https://doi.org/10.1016/j.marpetgeo.2015.02.011.

Wüest, A., Brooks, N.H., Imboden, D.M., 1992. Bubble plume modeling for lake restoration. Water Resour. Res. 28 (12), 3235–3250. https://doi.org/10.1029/92WR01681.

Zeebe, R.E., Wolf-Gladrow, 2001. CO_2 in Seawater: Equilibrium, Kinetics, Isotopes. Elsevier Oceanography Series, 65, Amsterdam, pp. 346.

Zheng, L., Yapa, P.D., 2002. Modeling gas dissolution in deep-water oil/gas spills. J. Mar. Syst. 31, 299–309.